Article

J. Braz. Chem. Soc., Vol. 23, No. 3, 415-425, 2012.
Printed in Brazil - ©2012 Sociedade Brasileira de Química
0103 - 5053 $6.00+0.00

Intercalation and Electrical Behavior of $Ta_xMo_{1-x}S_2$ ($x > 0.5$) Layered Mixed Disulfides

Nelson Lara,[,a] Pilar Aranda,[b] Ana I. Ruiz,[c] Víctor Manríquez[d] and Eduardo Ruiz-Hitzky[b]*

[a]*Departamento de Química, Universidad de Tarapacá, Av. General Velásquez 1775, Arica, Chile*

[b]*Instituto de Ciencia de Materiales de Madrid (ICMM-CSIC), Cantoblanco, 28049 Madrid, Spain*

[c]*Departamento de Geología y Geoquímica, Facultad de Ciencias, Universidad Autónoma de Madrid, Cantoblanco, 28049 Madrid, Spain*

[d]*Department of Chemistry, Faculty of Science, University of Chile, Las Palmeras 3427, Ñuñoa, Santiago, Chile*

Este trabalho relata um estudo sistemático do comportamento estrutural e elétrico de três fases ternárias do sistema $Ta_xMo_{1-x}S_2$ (x = 0,55, 0,75 e 0,90) e de seus compostos de intercalação resultantes das inserções química e eletroquímica de lítio, assim como das intercalações de piridina e poli(óxido de etileno). As três fases foram preparadas pela reação direta de seus elementos constituintes, sem qualquer outro aditivo, a 900 ºC em atmosfera inerte. Os compostos resultantes foram caracterizados por meio de difratometria de raios X de pó (XRD), análises termogravimétrica e térmica diferencial (TGA/DTA), fluorescência de raios X por dispersão de energia (EDX) e microscopia eletrônica de varredura com emissão de campo (FE-SEM). A condutividade elétrica dos diferentes compostos preparados foi medida no intervalo de temperatura 1,5-300 K utilizando o método convencional de sonda de quatro pontas van der Pauw na presença de um campo magnético de 9 T para verificar a ocorrência do fenômeno de magnetoresistividade.

This work reports a systematic study of the structural and electrical behavior of three ternary phases of the $Ta_xMo_{1-x}S_2$ system (x = 0.55, 0.75 and 0.90) and their intercalation compounds resulting from both chemical and electrochemical lithium insertions, as well as from pyridine and poly(ethylene oxide) intercalations. The three ternary phases were prepared by direct reaction of their constituting elements, without any other additive, at 900 ºC in inert atmosphere. The resulting compounds were characterized by means of X-ray powder diffractometry (XRD), thermogravimetric and differential thermal (TGA/DTA) analyses, energy dispersive X-ray fluorescence (EDX) and field emission-scanning electron microscopy (FE-SEM). The electrical conductivity of the different products was measured in the 1.5-300 K temperature range using the conventional four probe van der Pauw method in the presence of a 9 T magnetic field in order to verify the occurrence of magnetoresistivity phenomena.

Keywords: chalcogenides, intercalation, pyridine, PEO, conductivity

Introduction

The renewed interest to study layered solids is originated from the observation of unusual physical properties associated with anisotropy phenomena in such type of low-dimensional materials. Another important reason why 2D solids are investigated is their ability to intercalate a large variety of compounds.[1-9] In this context, physical properties such as electrical conductivity and electrochemical behavior of layered solids can be deliberately modified by intercalation of organic species.[2-4,10,11] Among different 2D solids, the study of layered transition-metal dichalcogenides (LTMDs) has become the subject of an active field of research in solid state physics and chemistry during the last decades.[1,12,13] One of the most salient physical properties of these materials is their electrical conductivity (and superconductivity) behavior, which is related to phase transitions usually driven by charge density wave mechanisms.[14] In general, LTMDs that include elements of the IV and VI groups are semiconductors, whereas

*e-mail: nlarah@uta.cl

those including elements belonging to the V group are metallic conductors, and even some of them, such as those containing Ta and Nb, may show superconductivity at low temperature.[15,16]

As known, the electrical properties of LTMDs can be modified by doping, provided that the doping element is compatible with the structure, yielding p- or n-type semiconductors according to the nature of the involved doping element.[17] Another way to modify the electrical properties of dichalcogenides is based on the introduction of metallic elements in the crystalline network, giving rise to mixed chalcogenides. In these compounds, distortion of the coordination polyhedra can take place. An example of this feature is the $Ta_xW_{1-x}Se_2$ solid solution, in which the structural changes happen as a function of the Ta/W ratio increase.[18]

Even for low tantalum contents (< 1%), significant changes can be observed in the electrical behavior, passing from semiconducting for WSe_2 to metallic conductivity in the $Ta_xW_{1-x}Se_2$ solid solution.[18] The idea of deliberately introduce changes in the electrical properties of WSe_2 either by doping or by synthesis of diverse mixed dichalcogenides has been also applied to other related LTMD systems. This is the case, for instance, of the TaS_2 system, in which the substitution of Ti for Ta stabilizes the octahedral 1*T* phase in the $Ti_xTa_{1-x}S_2$ solid solution presenting diamagnetism and semiconductivity as in the 1*T*-TaS_2 polytype.[19]

On the other hand, the intercalation of organic species into LTMDs has also been used to modify their electrical and electrochemical properties. The ability to accomplish direct intercalation of guest molecules into the van der Waals gap of dichalcogenides depends on the electronic structure of the concerned 2D host solid, as well as on the basicity (electron donor ability) of the guest species.[20] For instance, TaS_2, TiS_2 and $NbSe_2$ can directly intercalate nitrogen-containing compounds (ammonia, pyridine and other Lewis bases) as well as other polar molecules such as dimethyl sulfoxide (DMSO), triphenylphosphine, cobaltocene and aza-macrocyclic compounds.[21]

An alternative route, mainly applied to MoS_2, consists in the use of intermediate lithiated phases prepared by lithium chemical insertion using *n*-butyl lithium (*n*-BuLi).[6,7] These intermediate compounds are able to react with water producing colloidal dispersions due to the exfoliation of the dichalcogenide in elemental lamellae. In a further restacking process, these lamellae can entrap molecular or polymeric species present in the dispersion. In this way, polyoxyethylene compounds, such as crown-ethers and poly(ethylene oxide) (PEO), have been intercalated in MoS_2.[4,8,21-26] This approach implies an structural distortion that leads to a strong modification of the electronic structure of the host solid. As a consequence, the initial semiconducting MoS_2 becomes a metallic conductor due to the reduction produced by the *n*-BuLi.[27-29]

It is well known that group V LTMDs are superconductors with very low values of critical temperature (T_c) (*e.g.*, 2*H*-TaS_2: $T_c = 0.80$ K, 3*R*-$TaSe_2$: $T_c = 0.22$ K and 2*H*-$TaSe_2$: $T_c = 0.15$ K).[30-32] For an identical composition, different values for T_c can be observed depending on the nature of the dichalcogenide polytype, indicating the existence of a relationship between the superconducting behavior and the chalcogenide layer stacking. Interestingly, the intercalation of organic bases such as pyridine can introduce modifications of the superconducting behavior of such LTMD hosts.[33] This is the case for TaS_2, in which the intercalated pyridine injects electrons into the conduction band of the chalcogenide resulting in the modification of its electrical properties.[33] Keeping in mind that Mo and Ta are two elements showing very close atomic sizes (effective ionic radii: $Mo^{4+} = 0.084$ nm, $Ta^{4+} = 0.082$ nm)[34] and electronic configurations, it can be postulated that the profiles corresponding to the electronic band structure of Ta-Mo mixed dichalcogenides do not suffer dramatic changes for different composition ranges within a such solid solution. Theoretically, the conduction band of TaS_2 (d_z^2) can be filled by electrons from molybdenum as the Mo/Ta ratio increases in the mixed dichalcogenides. Ternary Ta-Mo sulfides were first described by Remmert *et al.*,[35,36] who reported their structural features with preliminary information on their conducting behavior and the possibility to intercalate compounds such as pyridine.

The aim of this work is to enhance the knowledge of these ternary compounds by investigating the electrical and electrochemical behaviors of various $Ta_xMo_{1-x}S_2$ phases, as well as of the derivatives resulting from their intercalation by different species: Li^+, pyridine and PEO. It should be noticed that $Ta_xMo_{1-x}S_2$ mixed chalcogenides can combine characteristics from both the semiconductor MoS_2 and the metallic TaS_2, which theoretically can be further modified by intercalation reactions.

Experimental

Synthesis of the $Ta_xMo_{1-x}S_2$ dichalcogenides

$Ta_xMo_{1-x}S_2$ dichalcogenides were synthesized by direct reaction from the corresponding elements (99.99% high purity powder for the metals and 98% for sulfur, both from Aldrich) at high temperature (900 ºC).[37,38] The elements were weighed and mixed at different stoichiometries in a glove box (MBRAUM MasterLab 130) with argon as inert atmosphere. The reactions were carried out in vacuum-sealed quartz ampoules (10^{-3} Torr). The synthesis was carried out in a two-step process: (*i*) the elements in

the quartz ampoules were thermally treated at a rate of 1 ºC min^{-1} to reach 600 ºC, maintaining this temperature for 5 days, and (*ii*) the recovered powder was pressed (4 ton cm^{-2}) to give pellets that were further heated at 900 ºC for 5 additional days. Samples were grounded in an agate mortar without control of the final particle size.

Lithium intercalation

Lithium chemical intercalation was performed on the basis of the Murphy's protocol[6] by reaction of the $Ta_xMo_{1-x}S_2$ dichalcogenides with *n*-BuLi (1.6 mol L^{-1} in hexane, Aldrich, 99% purity) for 24 h at 60 ºC, using 3 mol of Li *per* mol of dichalcogenide and operating under Ar atmosphere (dry glove box with a water content lower than 0.1 mg L^{-1}). The resulting dark products (lithiated phases) were recovered by centrifugation, washed with hexane several times and, finally, dried at room temperature in the dry glove box. The lithium determination was performed with a Plasma Emission ICP Spectrometer (Perkin Elmer, OPTIMA 2100 DV). Lithium electrochemical intercalation was typically carried out using the obtained dichalcogenides prepared as pellets (4 ton cm^{-2}) containing 50 mg of $Ta_xMo_{1-x}S_2$ agglomerated with methylene-propylene-diene monomer (EPDM) rubber (5% in weight) and dissolved in 3 mL cyclohexane containing 10% in weight of acetylene black (Super P from MMM Carbon) to produce the conducting dichalcogenide composites. These materials can act as positive electrodes, being able to insert lithium in the following electrochemical cell configuration: Li *per* 1 mol L^{-1} $LiClO_4$ in propylene carbonate (PC)/$Ta_xMo_{1-x}S_2$. The Li (Aldrich 3N5) negative electrodes were prepared as circular thin ribbons with the same diameter of the chalcogenide pellet (7 mm), being galvanostatically cycled in the range of 100-500 µA cm^{-2} and 1-4 V, using an EG&G PARC 273A galvanostat-potentiostat equipment.

Pyridine intercalation

Experiments with pyridine and the mixed chalcogenides are based on the method previously applied for the intercalation of such organic compound in other layered dichalcogenides.[33,39] The intercalation reaction was carried out in glass tubes (Pyrex R), where the dichalcogenides were intimately mixed with pure pyridine (Merck, 98%) in a 1:1 molar relationship. The ampoules were vacuum sealed by quenching the mixture by external immersion in liquid nitrogen and further maintained for 2 days at 150 ºC. After opening of the ampoule, the resulting product was separated by filtration, washed with isopropyl alcohol and finally dried in air at 25 ºC.

PEO intercalation

PEO was intercalated by treatment of the lithiated $Ta_xMo_{1-x}S_2$ phases following the same experimental approach used by our group for MoS_2 and TiS_2.[4,24] In this way, the lithiated phase was added to 1 mol L^{-1} aqueous solution of PEO (Merck > 98% purity; MW = 105 Da) and maintained under vigorous stirring for 24 h at 25 ºC. The resulting solid was recovered by centrifugation or filtration, repeatedly washed with water and finally vacuum-dried at 25 ºC.

Characterization techniques

The powder X-ray diffraction (XRD) measurements were carried out using PHILIPS PW 1710 and XPERT-MPD diffractometers, both equipped with a copper anode, a nickel filter and a graphite monochromator. Field emission-scanning electron microscopy (FE-SEM) images were recorded with a FEI NanoSEM Nova 230 microscope. This equipment is coupled to an EDAX Genesis XM2i analyzer used for punctual sampling and average analysis determinations (energy dispersive X-ray fluorescence, EDX). Thermogravimetric and differential thermal (TGA/DTA) analyses were performed under N_2 flux with a SEIKO SSC/5200 apparatus. The samples were placed in platinum capsules and heated from ambient temperature to 1000 ºC at a heating speed of 10 ºC min^{-1}.

Electrical conductivity measurements

The electrical conductivity was measured using the conventional four probes van der Pauw method[40] on the polycrystalline materials pressed as pellets (7 mm diameter with thickness between 1 and 3 mm). These measurements were carried out by applying a constant current of around 100 mV with a PPMS (Physical Properties Measurements System) apparatus that can operate with currents between 0.01 and 5000 µA, power between 0.001 to 1000 µW and temperature from 1.5 to 300 K. The measurements were also made in the presence of a 9 T magnetic field in order to investigate the occurrence of magnetoresistivity phenomena.

Results and Discussion

$Ta_xMo_{1-x}S_2$ dichalcogenides

Following the procedures described in the experimental section, several phases belonging to the $Ta_xMo_{1-x}S_2$ dichalcogenide system were synthesized by direct reaction

of precursors at 900 ºC. It was noticed that the addition of NH_4Cl was not necessary as preconized by Remmert *et al.*[35] in the first report on the preparation of these ternary sulfides. FE-SEM images of the resulting solids show the presence of micrometric crystals of hexagonal shape (Figure 1) with compositions that are in the range of the expected values, as deduced from EDX semiquantitative analysis.

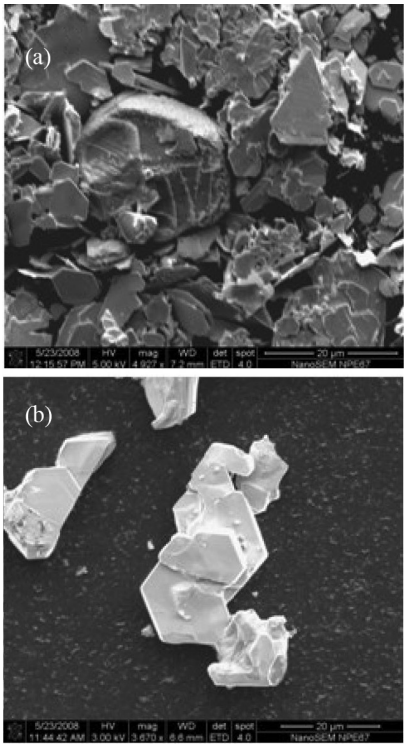

Figure 1. FE-SEM images of (a) $Ta_{0.75}Mo_{0.25}S_2$ and (b) $Ta_{0.90}Mo_{0.10}S_2$ dichalcogenides.

This work employed ternary phases in the $0.50 < x < 1.00$ composition range with x = 0.55, 0.75 and 0.90 because, according to Remmert *et al.*,[35] for compositions with x below *ca*. 0.50, a mixture of several phases of variable composition can be formed together with segregated MoS_2 crystals. In our case, pure phases of $Ta_xMo_{1-x}S_2$ seemed to be formed with $0.55 < x < 1.00$ in agreement with the XRD patterns shown in Figure 2. However, close examination of the profiles revealed the presence of a small number of extra reflections that could not be accounted for any supercell and were therefore assumed to be due to a low content of another phase, present as an impurity in the solid products.

From the diffractograms, the lattice parameters can be calculated ranging from 0.327 to 0.330 nm for the *a* axis and from 1.817 to 1.814 nm for the *c* axis, in good agreement with previous results for the 3*R*-$Ta_xMo_{1-x}S_2$ phases.[35] These results corroborate that the prepared dichalcogenides are present in a compact hexagonal structure, with the

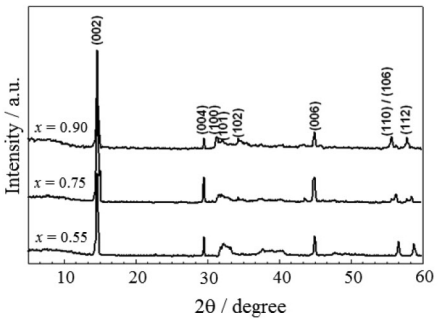

Figure 2. XRD powder patterns of the three prepared $Ta_xMo_{1-x}S_2$ dichalcogenides.

Ta and Mo metals in a trigonal prismatic coordination (3*R* polytype). As indicated above, the stabilization of such structural type is indicative of a metallic character, a result which was corroborated by the conductivity measurements performed at different temperatures (*vide infra*).

The high thermal stability of the synthesized dichalcogenides is deduced from DTA and TGA analyses (Figure S1 in Supplementary Information, SI), which indicate that there are not weight losses at temperatures below 500 ºC. The thermal stability moderately increases with the Ta content in the ternary dichalcogenides. As pointed out above, an interesting aspect of the partial Mo substitution in TaS_2 is the possibility of effectively modifying the electronic properties of the resulting mixed sulfides due to the modification of the electronic band structure. In this way, the ternary phases show notable increase of the electrical conductivity values when compared to those of the binary phases 2*H*-MoS_2 and 2*H*-TaS_2. Figure 3a shows the evolution of the electrical

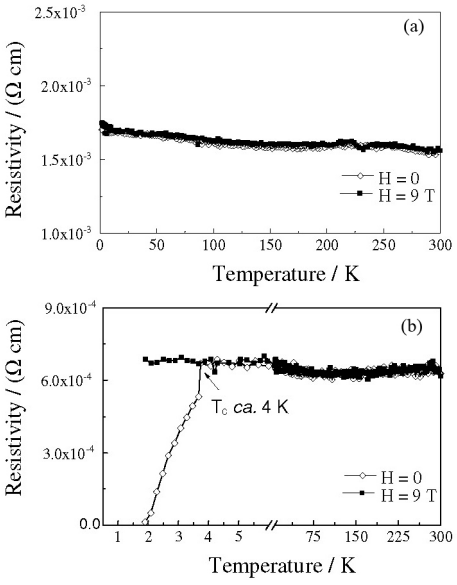

Figure 3. Resistivity-temperature curves for $Ta_xMo_{1-x}S_2$ dichalcogenides with (a) x = 0.55 and (b) x = 0.90, under H = 0 and H = 9 T magnetic fields.

resistance of $Ta_{0.55}Mo_{0.45}S_2$ in the 1.8-300 K range; a metallic behavior was observed with no dependence of the conductivity with the presence of an intense magnetic field (9 T). The resistivity (ρ) of this mixed sulfide phase is in the order of 10^{-3} Ω cm, much higher than that measured for MoS_2 (Table 1).

Table 1. Resistivity (Ω cm) at 298 K for various $Ta_xMo_{1-x}S_2$ phases

$Ta_xMo_{1-x}S_2$	Resistivity / (Ω cm)
$x = 0$	1.7×10^5
$x = 0.55$	1.4×10^{-3}
$x = 0.75$	5.0×10^{-3}
$x = 0.90$	6.3×10^{-4}
$x = 1.00$[41,42]	10^{-3}-10^{-4}

It can be postulated that the d_z^2 conduction band of TaS_2 accepts electrons from molybdenum, shifting the Fermi level to higher energy values and resulting in the observed metallic character of these materials. It is noteworthy that the $Ta_{0.9}Mo_{0.1}S_2$ phase presents an abrupt drop of resistance at very low temperature, *i.e.*, showing a superconducting behavior at T_c = 3.92 K (Figure 3b), a temperature that is much higher than that reported for TaS_2 (T_c = 0.8 K).[41] The measurements of the ternary phases with lower Ta content do not indicate superconductivity at least above T_c = 1.8 K, the lowest temperature that our conductivity measurement equipment can reach. The conductivity behavior of $Ta_{0.9}Mo_{0.1}S_2$ observed at very low temperature in either the presence or the absence of a strong magnetic field varies accordingly to the Meissner effect. From the magnetic ac susceptibility measurements, *ca.* 2% of the materials is in the superconducting state, which is an usual result for solids prepared as microcrystalline powders and measured as pressed pellets at relatively low-pressure,[42,43] as in the present case (4 ton cm^{-2}) (Figure S2 in SI).

Lithium insertion in $Ta_xMo_{1-x}S_2$ dichalcogenides

The ability of the $Ta_xMo_{1-x}S_2$ phases for the intercalation of electron donor species was tested by their reaction with both lithium and pyridine. Two experimental approaches, chemical and electrochemical, were applied for lithium intercalation. The first one is of particular interest because the intermediate compounds (lithiated phases) could be further used to prepare new inorganic-organic materials, similarly to that reported for MoS_2 and other disulfides.[4,8,21-25,44] The lithium chemical insertion (*i.e.*, the so-called lithiation reaction) was carried out by using *n*-BuLi, a method broadly used in intercalation chemistry.[6,7]

In the same way that observed for MoS_2, TaS_2 and other dichalcogenides (such as TiS_2 and ZrS_2),[45] lithiated phases of the ternary disulfides can be prepared. It is known that TaS_2 acts as a host lattice for lithium, reaching a maximum intercalation value of 1 mol of lithium *per* mol of dichalcogenide, whereas MoS_2 can intercalate up to 1.5 moles.[46] In the ternary phases, the maximum amount of intercalated lithium is close to 1 Li atom *per* formula unit (*i.e.*, $LiTa_xMo_{1-x}S_2$), being about 0.6 nm the increase of the interlayer distances in samples exposed to atmospheric moisture or washed with water. Hence, the intercalated lithium must be solvated by water molecules in a two-layer arrangement within the van der Waals region of the sulfide.

XRD patterns (Figure 4a) show less crystalline materials when compared to pristine disulfide, being in agreement with FE-SEM images that clearly indicate size reduction and alteration of the regular hexagonal shape of the microcrystals (Figure 4b). The alteration degree of the starting dichalcogenides is, however, below 10% of the total mass. This was determined by the chemical analysis of Mo and Ta present in the mother waters that were collected after washing of the lithiated phases.

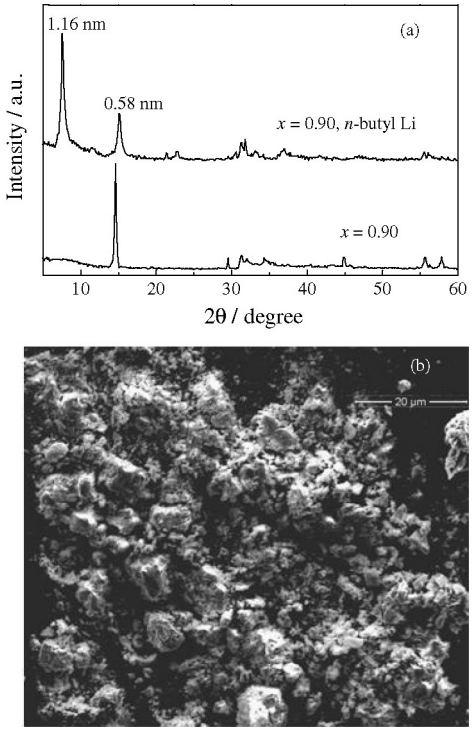

Figure 4. (a) XRD power patterns of $Ta_{0.90}Mo_{0.10}S_2$ before and after its treatment with *n*-BuLi and (b) FE-SEM image of the resulting $Li_{0.90}Ta_{0.90}Mo_{0.10}S_2$ material.

The lithium electrochemical intercalation was performed using a $Li/LiClO_4(PC)/Ta_xMo_{1-x}S_2$ cell configuration, in which Li-metal acted as negative electrode and $LiClO_4$

Table 2. Specific capacity (C_{spe}), voltage (V_m) and specific energy (E_{spe}) for the 1st and 2nd cycles of the Li/$LiClO_4$(PC)/$Ta_xMo_{1-x}S_2$ cells prepared with the three $Ta_xMo_{1-x}S_2$ dichalcogenides

Cell	1st cycle			2nd cycle		
Li/$LiClO_4$(PC)/$Ta_xMo_{1-x}S_2$	C_{spe} / (Ah kg^{-1})	V_m / V	E_{spe} / (Wh kg^{-1})	C_{spe} / (Ah kg^{-1})	V_m / V	E_{spe} / (Wh kg^{-1})
$x = 0.55$	142	2.0	284	114	2.0	228
$x = 0.75$	107	2.4	259	97	2.4	235
$x = 0.90$	122	2.0	244	113	2.0	226

dissolved in PC was employed as electrolyte. Discharge curves with two steps were observed (Figure 5), which could be tentatively ascribed to the partial reduction of both Mo and Ta transition metals. The voltage value decreased to *ca*. 1.4 V followed by a plateau at *ca*. 1.3 V as the amount of intercalated Li *per* formula (y) increased, reaching a maximum value of about 1 unit (y = 1, Table 2).

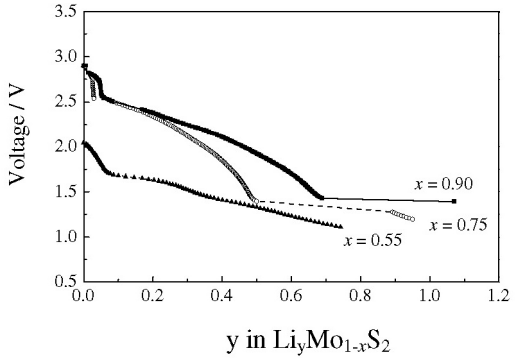

Figure 5. Voltage *vs.* proportion of intercalated Li (y) in the $Ta_xMo_{1-x}S_2$ dichalcogenides ($x = 0.55$, 0.75 and 0.90).

Similar behavior towards Li intercalation in TaS_2 was reported by Thompson.[47] Cycling experiments of electrochemical cells using the $Ta_xMo_{1-x}S_2$ phases with $x > 0.50$ as cathodes show specific capacity values in the 100-140 Ah kg^{-1} range during the first cycle (cell discharge). These values are inferior to those reported for other chalcogenides such as MoS_2 and TiS_2, which show capacity values of 160 and 225 Ah kg^{-1} respectively.[48] The successive charge/discharge cycles produce a 10-20% decrease of the specific capacity, and, in general, low reversibility in the electrochemical process of the Li insertion is observed.[43] In conclusion, these results show the possibility of electrochemical insertion of Li in the $Ta_xMo_{1-x}S_2$ ternary phases, but they are also indicative of their scarce practical application as electrodes of rechargeable Li-batteries.

Pyridine-$Ta_xMo_{1-x}S_2$ intercalation compounds

The $Ta_xMo_{1-x}S_2$ ($x > 0.5$) mixed chalcogenides can intercalate pyridine by treatment at 150 ºC for 48 h, reaching an intercalation maximum of *ca.* 0.5 molecule of pyridine *per* dichalcogenide formula, as deduced from elemental analyses and thermogravimetric curves (Table 3). It should be noted that pyridine cannot be intercalated into MoS_2, whereas about 0.5 mol *per* mol is effectively intercalated in the TaS_2 binary dichalcogenide, in the same way that observed here for the $Ta_xMo_{1-x}S_2$ ternary phases.[39]

Table 3. Chemical formulae deduced from chemical analyses and weight loss values obtained from the TGA curves for the pyridine intercalation compounds

$Ta_xMo_{1-x}S_2$	Intercalation compound	TGA / %, weight loss	
		Calculated	Experimental
$x = 0.55$	$Ta_{0.55}Mo_{0.45}S_2 \cdot 0.32Py$	10.9	11.5
$x = 0.75$	$Ta_{0.75}Mo_{0.25}S_2 \cdot 0.41Py$	12.6	10.9
$x = 0.90$	$Ta_{0.90}Mo_{0.10}S_2 \cdot 0.46Py$	13.3	12.5

As accounted for the TaS_2 intercalation compound, pyridine acts as a Lewis base, and the electrons from the N atom can be transferred to the conduction band of the sulfide. Remmert and Hummel[36] reported similar intercalation rates in experiments involving several $Ta_xMo_{1-x}S_2$ phases that were treated with pyridine under more drastic conditions (14 days at 200 ºC). These authors proposed a two-step mechanism for the intercalation process, observing changes in the stacking sequence of the host lattice. In the present work, the XRD patterns of Figure 6 show a shift of the [00l] reflections from 0.60 to 1.21 nm due to the interlayer expansion that takes place by

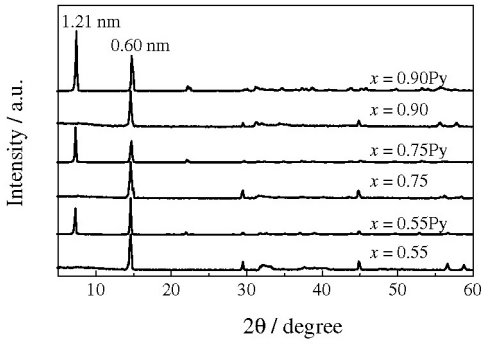

Figure 6. XRD powder patterns of the $Ta_xMo_{1-}xS_2$ dichalcogenides ($x = 0.55$, 0.75 and 0.90) before and after pyridine intercalation (Py).

Table 4. Results of chemical analysis (C and N contents) and basal spacing values for different dichalcogenides after pyridine intercalation

Chalcogenides treated with pyridine	Elemental analysis		*c* / nm	Δ*c* / nm
	C / %	N / %		
MoS_2	0.02	0.01	0.615	0.000
$Ta_{0.55}Mo_{0.45}S_2 \cdot 0.32Py$	8.41	1.79	1.205	0.600
$Ta_{0.75}Mo_{0.25}S_2 \cdot 0.41Py$	9.39	2.01	1.205	0.600
$Ta_{0.90}Mo_{0.10}S_2 \cdot 0.46Py$	10.09	2.17	1.192	0.590
$TaS_2 \cdot 0.5Py$[45]	10.48	2.60	1.206	0.601

incorporation of pyridine into the van der Waals gap of the dichalcogenide, in a similar way as reported for TaS_2.[36,39]

Table 4 summarizes the compositions and interlayer expansions deduced from chemical analyses and diffractograms, respectively, for pyridine intercalation in the three studied phases of the ternary dichalcogenides. The pyridine insertion provokes an increase of the *c* parameter of *ca.* 0.6 nm, which could be interpreted by assuming that the pyridine molecule adopts an orientation with the ring plane perpendicular to the plane defined by the layers of the solid hosts (Figure 7a). A similar orientation of pyridine, in which the nitrogen heteroatom is located in the center of the interlayer space between two chalcogenide sheets, was assigned by Wadas *et al.*[49] to $NbS_2 \cdot 0.5Py$, from neutron diffraction data produced by a single crystal of this pyridine-dichalcogenide intercalation compound.[49] Besides, a similar disposition was also assumed for other layered dichalcogenides such as TaS_2,[50] also supporting the current proposed arrangement of this guest molecule in the interlayer region of the studied ternary phases.

The pyridine intercalation in $Ta_xMo_{1-x}S_2$ is a reversible process, as indicated by the spontaneous and progressive loss of the guest molecules taking place after sample exposition for several days to the atmosphere at room temperature. DTA and TGA analyses of $Ta_xMo_{1-x}S_2 \cdot n$Py carried out under N_2 flow indicate that the pyridine desorption occurs in two steps at temperatures lower than 300 ºC. A similar behavior was also observed for $TaS_2 \cdot 0.5Py$.[51] This behavior suggests that the involved host-guest interaction mechanism could be comparable in both types of solids, *i.e.*, for binary TaS_2 and the ternary dichalcogenides. According to Schöllhorn *et al.*,[52] a plausible interpretation of such behavior could be based on the role of pyridine in the reduction of Ta^{IV} giving bipyridine (Py-Py) and pyridinium cations (Py-H^+). The $Ta_xMo_{1-x}S_2 \cdot n$Py intercalation compounds treated at 100 ºC under nitrogen flow show a decrease in the intensity of the XRD [00l] reflections after 15 min of treatment (Figure 8b), that completely disappear after 30 min of heating (Figure 8c). The resulting solid shows lower crystallinity when compared to the pristine dichalcogenide (Figure 8d). This is in good agreement with FE-SEM images of deintercalated samples that show alterations and cracking of particles due to the action of *n*-BuLi on the microcrystals of the intercalated solids (Figure 7b).

The electrical resistivity of $Ta_xMo_{1-x}S_2 \cdot n$Py intercalation compounds is higher than those of the pristine dichalcogenides and increases with the pyridine content

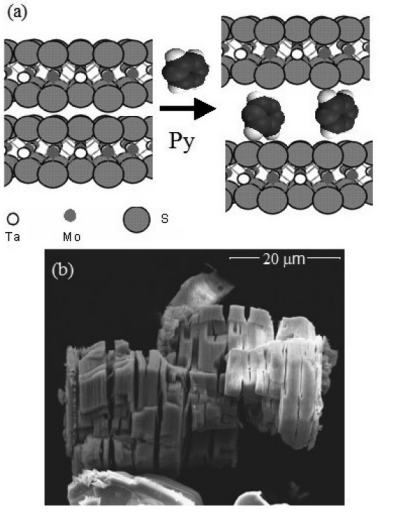

Figure 7. (a) Schematic representation of the pyridine (Py) insertion in the $Ta_xMo_{1-x}S_2$ dichalcogenides and (b) FE-SEM image of the intercalated $Ta_{0.90}Mo_{0.10}S_2 \cdot 0.46$Py sample.

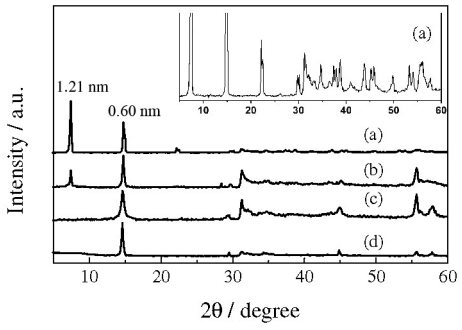

Figure 8. XRD powder patterns of the $Ta_{0.90}Mo_{0.10}S_2 \cdot 0.46$Py intercalated compound: (a) as obtained and after heating at 100 ºC for (b) 15 and (c) 30 min, and (d) the $Ta_{0.90}Mo_{0.10}S_2$ dichalcogenide. The inset corresponds to a magnification of the (a) diffractogram showing peaks at the highest values of 2θ.

(Table 5), showing a semiconducting behavior according to the resistivity variation with temperature (Figure S3 in SI). Interestingly, in addition to the semiconducting behavior observed in a wide range of temperatures, the $Ta_{0.9}Mo_{0.1}S_2$·0.46Py phase shows superconducting properties with a T_c value close to 4 K, similar to that of the pristine dichalcogenide (Figure S3 in SI). It should be noted that this is one of the few organic-inorganic systems known exhibiting superconductivity behavior.

Table 5. Resistivity (Ω cm) values measured at 298 K for the $Ta_xMo_{1-x}S_2$ phases and their corresponding pyridine intercalation compounds

Compound	Resistivity / (Ω cm)
$Ta_{0.55}Mo_{0.45}S_2$	1.4×10^{-3}
$Ta_{0.55}Mo_{0.45}S_2$·0.32Py	2.7×10^{-1}
$Ta_{0.75}Mo_{0.25}S_2$	5.0×10^{-3}
$Ta_{0.75}Mo_{0.25}S_2$·0.41Py	2.3×10^{-2}
$Ta_{0.90}Mo_{0.10}S_2$	6.3×10^{-4}
$Ta_{0.90}Mo_{0.10}S_2$·0.46Py	3.8×10^{-2}

PEO-$Ta_xMo_{1-x}S_2$ nanocomposites

PEO can be intercalated into the $Ta_xMo_{1-x}S_2$ ternary phases following a similar approach to that previously reported for MoS_2 and TiS_2 via the corresponding lithiated phases.[8,24] The reaction of the $LiTa_xMo_{1-x}S_2$ intermediate phases with aqueous solutions of PEO produces a colloidal dispersion of the elemental lamellae of the selected ternary dichalcogenide (exfoliated $Ta_xMo_{1-x}S_2$) intimately mixed with the polymer that can be recovered by centrifugation. This last process produces the re-stacking of the exfoliated dichalcogenide constituted by the pristine sulfide sheets to which PEO can associate, giving nanocomposite materials. Strictly speaking, it should be considered that the whole process consists in an entrapping procedure better than an intercalation phenomenon. In fact, the chalcogenide lattices are irreversibly modified during the redox reaction of the lithiated phases with the water molecules.

Table 6 summarizes the chemical compositions of PEO/Ta-Mo disulfide composites deduced from the elemental analyses after water washing and vacuum-drying at room temperature. These show that *ca.* 2 mol of PEO *per* dichalcogenide formula are assembled into the inorganic host lattice. The obtained dark solids were characterized by XRD and the corresponding patterns show new [00l] reflections indicating a shift of the *c* parameter from 0.605 nm to *ca.* 1.6 nm, although low intensity peaks related to a second phase can be also observed (Figure 9).

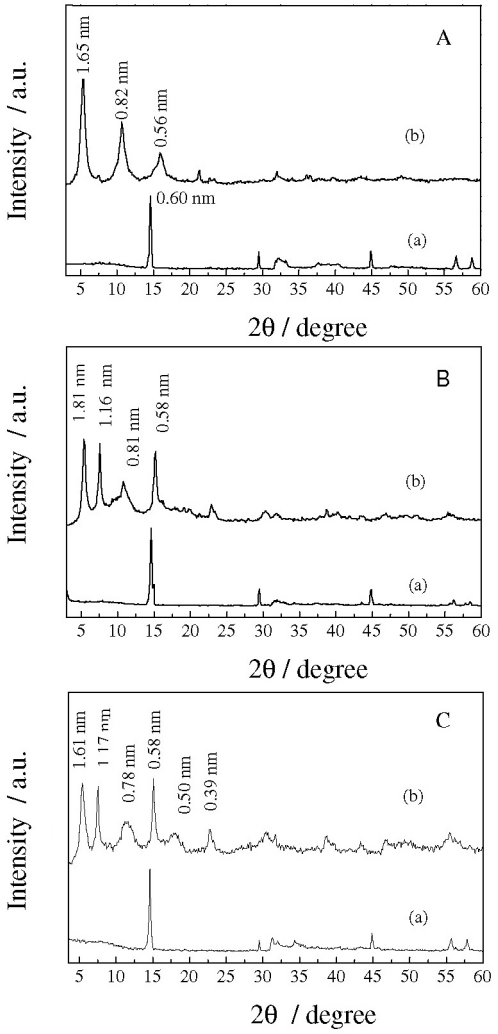

Figure 9. XRD powder patterns of: (A) $Ta_{0.55}Mo_{0.45}S_2$ (a) and $Li_{0.97}Ta_{0.55}Mo_{0.45}S_2$·2.3PEO (b), (B) $Ta_{0.75}Mo_{0.25}S_2$ (a) and $Li_{0.96}Ta_{0.75}Mo_{0.25}S_2$·1.8PEO (b) and (C) $Ta_{0.90}Mo_{0.10}S_2$ (a) and $Li_{0.95}Ta_{0.90}Mo_{0.10}S_2$·2.2PEO (b).

Table 6. Formulae deduced from chemical analyses and basal spacing values in the three studied $Ta_xMo_{1-x}S_2$ dichalcogenides intercalated with PEO from their lithiated phases

Host $Ta_xMo_{1-x}S_2$ dichalcogenide	Basal spacing value			Intercalation compound
	c_0 / nm	c / nm	Δc / nm	Lithiated phase
$x = 0.55$	0.605	1.61	1.00	$Li_{0.97}Ta_{0.55}Mo_{0.45}S_2$·2.3PEO
$x = 0.75$	0.605	1.63	1.04	$Li_{0.96}Ta_{0.75}Mo_{0.25}S_2$·1.8PEO
$x = 0.90$	0.605	1.61	1.00	$Li_{0.95}Ta_{0.90}Mo_{0.10}S_2$·2.2PEO

Table 7. Resistivity (Ω cm) values measured at 298 K, electrical behavior (between 1.8 and 300 K) and activation energy (eV) for the $Ta_xMo_{1-x}S_2$ phases, their pyridine intercalation compounds and their PEO nanocomposites

Compound	Resistivity / (Ω cm)	Electrical behavior	Activation energy / eV
$Ta_{0.55}Mo_{0.45}S_2$	1.4×10^{-3}	metal	–
$Ta_{0.55}Mo_{0.45}S_2$·0.32Py	2.7×10^{-1}	semiconductor	1.2×10^{-4}
$Ta_{0.75}Mo_{0.35}S_2$	5.0×10^{-3}	metal	–
$Ta_{0.75}Mo_{0.35}S_2$·0.41Py	2.3×10^{-2}	semiconductor	4.9×10^{-4}
$Ta_{0.90}Mo_{0.10}S_2$	6.3×10^{-4}	metal (T > 4 K)	–
		superconductor (T_c = 4 K)	
$Ta_{0.90}Mo_{0.10}S_2$·0.46Py	3.8×10^{-2}	semiconductor (T > 4 K)	4.9×10^{-4}
		superconductor (T_c = 4 K)	
$Ta_{0.90}Mo_{0.10}S_2$·1.8PEO	1.93	semiconductor	1.7×10^{-3}
$Ta_{0.90}Mo_{0.10}S_2$·2.2PEO	208.5	semiconductor	1.0×10^{-3}

This basal spacing increase of *ca.* 1 nm can be attributed to the presence of the polymer entrapped between the dichalcogenide layers during the re-stacking process. It has been postulated for PEO intercalation compounds in transition-metal sulfides and other host solids such as silicates and vanadium pentoxide xerogels that the polymer can be arranged in the interlayer space of the 2D solid either with double-layer (zig-zag conformation) or with helical configuration of more or less distorted polyoxyethylene chains.[53-58] The observed increase of the basal spacing in these materials is *ca.* 0.8 nm and, in some cases, the PEO chains in monolayer disposition produce a basal spacing increase of *ca.* 0.4 nm. In the present case, in addition to the above-mentioned reflections at *ca.* 1.6 nm that could be assigned to the presence of either helical or double-layer PEO chains, there are also diffraction peaks at 1.16 and 0.58 nm that may be related to the pristine chalcogenide. However, these peaks could also be tentatively ascribed to the 1st and 2nd rational reflections, respectively, of the layered solid with PEO in a monolayer disposition (Figures 9b and 9c). Additionally, the possible presence of hydrated Li^+ and OH^- species produced during the reactions of the lithiated phases with water should also be considered, as they too can contribute to the sulfide interlayer expansion. In this way, it is difficult at this stage to distinguish the contribution of the different species in the observed mixed-dichalcogenide layer expansion, although the presence of OH^- species may favor distortions in the highly stable PEO helicoidal structure.

The electrical characterization of the PEO intercalated compounds *vs.* temperature (1.8-300 K) indicates that these materials are semiconductors with typical resistivity values of ρ = 0.27, ρ = 1.93 and ρ = 208.50 Ω cm for PEO-$Ta_xMo_{1-x}S_2$ nanocomposites with x = 0.55, 0.75 and 0.90, respectively (Figure S4 in SI). Table 7 lists the electrical characteristics of the studied ternary phases as well as their intercalation compounds with pyridine and PEO. In general, an increase of the resistivity is observed with the incorporation of the polymer, changing, in some cases, the metallic character inherent to the pristine chalcogenides to a semiconducting behavior in the corresponding intercalated phases.

Conclusions

$Ta_xMo_{1-x}S_2$ ternary phases with x = 0.55, 0.75 and 0.90 exhibit intermediate characteristics when compared to the two related binary phases, *i.e.*, TaS_2 and MoS_2. The mixed sulfides present a 3*R*-type compact hexagonal structure with the transition metals in trigonal prismatic coordination, showing metallic electrical conductivity as reported for TaS_2.[41] Moreover, the $Ta_{0.90}Mo_{0.10}S_2$ phase behaves as a superconductor with T_c = 4 K. Like MoS_2 and other disulfides, the ternary chalcogenides are able to insert lithium by chemical and electrochemical pathways, but, despite the reversible insertion of Li into the $Ta_xMo_{1-x}S_2$ ternary phases, their electrochemical characteristics are not advantageous for practical use as electrodes of rechargeable Li-batteries, when compared to other chalcogenides.

The possibility of inserting lithium by using *n*-BuLi is of particular interest because the intermediate lithiated phases could be further used to prepare new organic-inorganic materials, such as PEO-LTMD nanocomposites, similarly to that reported for MoS_2 and TiS_2.[8,24] The incorporation of this polymer changes, in some cases, the metallic character inherent to the pristine chalcogenides to a semiconducting behavior. The mixed dichalcogenides are also able to directly insert pyridine. Interestingly, the $Ta_{0.90}Mo_{0.10}S_2$·0.46Py intercalation compound presents superconductivity with a value of T_c = 4 K, being one of

the few reported organic-inorganic systems that show this type of behavior.

Supplementary Information

Supplementary data are available free of charge at http://jbcs.sbq.org.br as a pdf file.

Acknowledgments

This work has been partially supported by the CICYT (Spain, project MAT2006-03356) and by the Convenio de Desempeño UTA – Mineduc (Chile). Authors thank Mr. A. Valera for technical assistance in the FE-SEM and EDX studies. Dr. Nelson Lara also thanks the Spanish Ministry of Foreign Affaires for a Mutis fellowship.

References

1. Whittingham, M. S.; Ebert, L. B. In *Intercalated Layered Materials*; Levy, F., ed.; D. Reidel Publishing Co.: Dordrecht, Holland, 1979.
2. Schollhorn, R.; *Angew. Chem., Int. Ed. Eng.* **1980**, *19*, 983.
3. Kanatzidis, M. G.; Tonge, L. M.; Marks, T. J.; Marcy, H. O.; Kannewurf, C. R.; *J. Am. Chem. Soc.* **1987**, *109*, 3797.
4. Ruiz-Hitzky, E.; *Adv. Mater.* **1993**, *5*, 334.
5. Villanueva, A.; Ruiz-Hitzky, E.; *J. Mater. Chem.* **2004**, *14*, 824.
6. Murphy, D.; Christian, P. A.; Disalvo, F.; Waszczak, J.; *Inorg. Chem*. **1976**, *15*, 17.
7. Dines, M.; *Mater. Res. Bull.* **1975**, *10*, 287.
8. Ruiz-Hitzky, E.; Jimenez, R.; Casal, B.; Manriquez, V.; Santa Ana, A.; Gonzalez, G.; *Adv. Mater.* **1993**, *5*, 738.
9. Santa Ana, M.; Mirabal, M.; Benavente, E.; Gomez-Romero, P.; Gonzalez, G.; *Electrochim. Acta* **2007**, *53*, 1432.
10. Leroux, F.; Koene, B. E.; Nazar, L. F.; *J. Electrochem. Soc.* **1996**, *143*, L181.
11. Gomez-Romero, P.; *Adv. Mater.* **2001**, *13*, 163.
12. Whittingham, M. S.; *Prog. Solid State Chem.* **1978**, *12*, 41.
13. Whittingham, M. S.; Jacobson, A. J. In *Intercalation Chemistry*; Whittingham, M. S.; Jacobsen, A. J., eds.; Academic Press: New York, USA, 1982.
14. Mattheiss, L. F.; *Phys. Rev. B: Condens. Matter Mater. Phys.* **1973**, *8*, 3719.
15. Fang, L.; Wang, Y.; Zou, P. Y.; Tang, L.; Xu, Z.; Chen, H.; Dong, C.; Shan, L.; Wen, H. H.; *Phys. Rev. B: Condens. Matter Mater. Phys.* **2005**, *72*, 14534-1.
16. Katayama, N.; *Phys. C* **2006**, *445*, 35.
17. Brixner, L. H.; *J. Electrochem. Soc.* **1963**, *110*, 289.
18. Hicks, W. T.; *J. Electrochem. Soc.* **1964**, *111*, 1058.
19. Thompsom, A. H.; Gamble, F. R.; Koehler Jr., R. F.; *Phys. Rev. B: Condens. Matter Mater. Phys.* **1972**, *5*, 2811.
20. Rao, G. V. S.; Shafer, M. W. In *Intercalated Layered Materials*; Levy, F., ed.; D. Reidel Publishing Co.: Dordrecht, Holland, 1979.
21. Bissessur, R.; Kanatzidis, M. G.; Schindler, J. L.; Kannewurf, C. R.; *J. Chem. Soc., Chem. Commun.* **1993**, 1582.
22. Lemmon, J. P.; Lerner, M. M.; *Chem. Mater.* **1994**, *6*, 207.
23. Lara, N.; Ruiz-Hitzky, E.; *J. Braz. Chem. Soc.* **1996**, *7*, 193.
24. Gonzalez, G.; Santa Ana, M. A.; Benavente, E.; *Electrochim. Acta* **1998**, *43*, 1327.
25. Ruiz-Hitzky, E.; Aranda, P. In *Polymer-Clay Nanocomposites*; Pinnavaia, T. J.; Beall, G. W., eds.; John Willey & Sons: West Sussex, UK, 2000.
26. Benavente, E.; Santa Ana, M. A.; Gonzalez, G.; *Phys. Status Solidi B* **2004**, *241*, 2444
27. Chrissafis, K.; Zamani, M.; Kambas, K.; Stoemenos, J.; Economou, N. A.; Sameras, I.; Julien, C.; *Mater. Sci. Eng., B* **1989**, *3*, 145.
28. Wypych, F.; Schollhorn, R.; *J. Chem. Soc., Chem. Commun.* **1992**, 1386.
29. Heising, J.; Kanatzidis, M. G.; *J. Am. Chem. Soc.* **1999**, *121*, 11720.
30. Smith, T.; Shelton, R.; Schwall, R.; *J. Phys. F: Metals Phys.* **1975**, *5*, 1713.
31. Di Salvo, F. J.; Moncton, D. E.; Wilson, J.; Mahajans, J. ; *Phys. Rev. B: Condens. Matter Mater. Phys.* **1976**, *14*, 1543.
32. Revolinsky, R.; Beerntsen, D.; *J. Phys. Chem. Solids* **1966**, *27*, 523.
33. Gamble, G.; Disalvo, F. J.; Klemm, R. A.; Geballe, T.; *Science* **1970**, *168*, 568.
34. Gamble, F. R.; *J. Solid State Chem.* **1974**, *9*, 358.
35. Remmert, P.; Fischer, E.; Hummel, H.-U.; *Z. Naturforsch., B: Chem.* **1994**, *49b*, 1175.
36. Remmert, P.; Hummel, H.-U.; *Z. Naturforsch., B: Chem.* **1994**, *49b*, 1387.
37. McTaggart, K. F.; Wadsley, E.; *Aust. J. Chem.* **1958**, *11*, 445.
38. Jellinek, F.; *J. Less-Commom Met.* **1962**, *4*, 9.
39. Gamble, F. J.; Osiecki, J. H.; Disalvo, F. J.; *J. Chem. Phys.* **1971**, *55*, 3525.
40. van der Pauw, L. J.; *Philips Res. Rept.* **1958**, *13*, 1.
41. Murphy, D. W.; Christian, P. A.; *Science* **1979**, *205*, 651.
42. Thompson, A. H.; *Physics* **1980**, *99B*, 100.
43. Gamble, F.; Osiecki, J.; Cais, M.; Pisharody, R.; Disalvo, F. J.; Geballe, T. H.; *Science* **1971**, *174*, 493.
44. Jorgensen, J. D.; Dabrowski, B.; Pei, S. Y.; Hinks, D. G.; Soderholm, L.; Morosin, B.; Schirber, J. E.; Venturini, E. L.; Ginley, D. S.; *Phys. Rev. B: Condens. Matter Mater. Phys.* **1988**, *38*, 11337.
45. Lara, N.; *Síntesis, Caracterización, Propiedades Eléctricas y de Intercalación de Calcogenuros Mixtos Laminares*; Thesis (PhD), Biblioteca Universidad Complutense, Química Inorgánica- Tesis Ineditas, clasificación 546(043.2) Madrid, 1996; document or data available from author upon request.

46. Kanatzidis, M.; Bissessur, R.; De Groot, D.; Schindler, J. L; Kannewurf, C. R.; *Chem. Mater.* **1993**, *5*, 595.
47. Whittingham, M. S.; Gamble Jr., F. R.; *Mater. Res. Bull*. **1975**, *10*, 363.
48. Julien, C.; Nazrri, G.; *Solid State Batteries: Materials Design and Optimization*; Kluwer Academic Publishers: Massachusetts, USA, 1994.
49. Wadas, S.; Alloul, H.; Molinie, P.; *J. Phys. Lett.* **1978**, *39*, L243.
50. Jacobson, J. A. In *Solid State Chemistry Compounds*; Cheetham, A. K.; Day, P., eds.; Clarendon Press: Oxford, 1992, ch. 6.
51. Thompson, A. H.; *Nature* **1974**, *251*, 492.
52. Schöllhorn, R.; Zagefha, H.; Butz, T.; Lerf, A.; *Mater. Res. Bull.* **1979**, *14*, 369.
53. Ruiz-Hitzky, E.; Aranda, P.; *Adv. Mater.* **1990**, *2*, 545.
54. Aranda, P.; Ruiz-Hitzky, E.; *Chem. Mater.* **1992**, *4*, 1395.
55. Ruiz-Hitzky, E.; Aranda, P.; Casal, B.; *J. Mater. Chem.* **1992**, *2*, 581.
56. Aranda, P.; Ruiz-Hitzky, E.; *Acta Polym*. **1994**, *45*, 59.
57. Ruiz-Hitzky, E.; Aranda, P.; Casal, B.; Galvan, J. C.; *Adv. Mater.* **1995**, *7*, 180.
58. Ruiz-Hitzky, E.; Aranda, P.; *An. Quim., Int. Ed.* **1997**, *93*, 197.

Submitted: May 19, 2011
Published online: January 10, 2012